Competition of Dzyaloshinskii-Moriya and Higher-Order Exchange Interactions in Rh/Fe Atomic Bilayers on Ir(111)

Niklas Romming,[1] Henning Pralow,[2] André Kubetzka,[1] Markus Hoffmann,[2,3] Stephan von Malottki,[2] Sebastian Meyer,[2] Bertrand Dupé,[2,4] Roland Wiesendanger,[1] Kirsten von Bergmann,[1,*] and Stefan Heinze[2]

[1]*Department of Physics, University of Hamburg, 20355 Hamburg, Germany*

[2]*Institut für Theoretische und Astrophysik, Christian-Albrechts-Universität zu Kiel, 24098 Kiel, Germany*

[3]*Peter Grünberg Institut and Institute for Advanced Simulation, Forschungszentrum Jülich and JARA, 52425 Jülich, Germany*

[4]*Institute of Physics, Johannes Gutenberg-Universität Mainz, Staudingerweg 7, 55128 Mainz, Germany*

(Received 2 November 2017; revised manuscript received 27 February 2018; published 14 May 2018)

Using spin-polarized scanning tunneling microscopy and density functional theory we demonstrate the occurrence of a novel type of noncollinear spin structure in Rh/Fe atomic bilayers on Ir(111). We find that higher-order exchange interactions depend sensitively on the stacking sequence. For fcc-Rh/Fe/Ir(111), frustrated exchange interactions are dominant and lead to the formation of a spin spiral ground state with a period of about 1.5 nm. For hcp-Rh/Fe/Ir(111), higher-order exchange interactions favor an up-up-down-down (↑↑↓↓) state. However, the Dzyaloshinskii-Moriya interaction at the Fe/Ir interface leads to a small angle of about 4° between adjacent magnetic moments resulting in a canted ↑↑↓↓ ground state.

DOI: 10.1103/PhysRevLett.120.207201

In systems with broken inversion symmetry and strong spin-orbit coupling (SOC), the Dzyaloshinskii-Moriya interaction (DMI) [1,2] plays an essential role for the formation of topologically nontrivial spin structures such as Skyrmions [3–10]. At transition-metal surfaces and interfaces the DMI can induce numerous types of noncollinear spin structures such as cycloidal spin spirals [11–13], Néel-type domain walls [14–19], as well as Skyrmions and Skyrmion lattices [20–27].

In such systems there is a competition between the DMI favoring a noncollinear spin structure and the Heisenberg exchange, which typically favors collinear alignment of magnetic moments. Depending on their strength and the magnetocrystalline anisotropy energy, a spin spiral state forms in zero magnetic field and a transition to Skyrmions occurs at finite field. However, higher-order exchange interactions such as the four-spin or biquadratic term can lead to more complex spin structures, e.g., multi-Q states [28], conical spin spirals [29], or atomic-scale spin lattices [20,30]. For an Fe monolayer on Rh(111) a so-called up-up-down-down (↑↑↓↓) state has been predicted [31,32] based on density functional theory (DFT); however, it has not been observed experimentally yet.

Here, we demonstrate that the interplay of DMI and higher-order exchange can lead to the formation of a novel type of canted ↑↑↓↓ state, with small angles between adjacent magnetic moments. We study atomic Rh/Fe bilayers on the Ir(111) surface which grow pseudomorphically, as shown by scanning tunneling microscopy (STM) measurements. While Fe grows in fcc stacking only, both hcp and fcc stacking of Rh are observed. The ground state spin structure of the film depends on the stacking of the Rh overlayer. In the fcc stacking we observe a spin spiral state in spin-polarized (SP-)STM images with a period of 1.5 nm, which is driven by the frustration of exchange interactions, as shown from DFT calculations. For the hcp-Rh stacking, we show based on DFT that higher-order exchange favors an ↑↑↓↓ state. The significant DMI at the Fe/Ir interface leads to a small canting of the magnetic moments. Spin-polarized STM measurements with different tip magnetization directions are in agreement with this noncollinear spin structure.

A STM measurement of a typical Rh/Fe/Ir(111) sample is shown in Fig. 1(a), where the color coding refers to the local differential conductance (dI/dU) (see Ref. [33] for the sample preparation). At this bias voltage, Fe and Ir have similar dI/dU signals, but there are two clearly distinguishable contrast levels for the Rh islands. The signal strength correlates with the orientation of the roughly triangular Rh islands, a sign of pseudomorphic growth of Rh with both possible stackings exhibiting slightly different electronic properties. We assign the darker dI/dU signal at this bias voltage to fcc-Rh and the brighter one to hcp-Rh (see Ref. [33] for details).

In order to investigate the structural, electronic, and magnetic properties of such atomic Rh/Fe bilayers on the Ir(111) surface, we have performed DFT calculations using the FLEUR code (see Ref. [33] for computational details). We start by discussing the energy dispersion $E(\mathbf{q})$ of flat homogeneous spin spirals obtained without taking SOC into account [black data in Fig. 1(b)]. The energy dispersions show that the ferromagnetic (FM) state at $\bar{\Gamma}$ has lower energy than the antiferromagnetic (AFM) states at the Brillouin zone boundary. For both Rh stackings there are

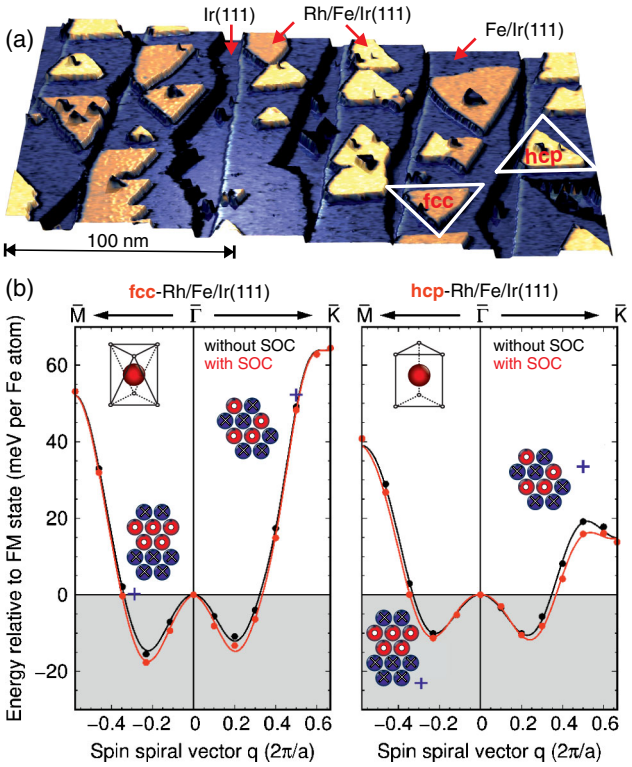

FIG. 1. (a) Perspective STM constant-current image of a typical Rh/Fe/Ir(111) sample with approximately 0.8 ML Fe and 0.4 ML Rh, colorized with the simultaneously acquired dI/dU signal ($U = +0.5$ V, $I = 0.75$ nA, $T = 8$ K). (b) Calculated energy dispersions $E(\mathbf{q})$ of right-rotating cycloidal homogeneous spin spirals for fcc-Rh (left) and hcp-Rh (right) on Fe/Ir(111) without spin-orbit coupling (black symbols) and with spin-orbit coupling (red symbols). The lines denote fits to the Heisenberg model including the Dzyaloshinskii-Moriya interaction for the case with spin-orbit coupling (see Ref. [33] for details). The energies of the $\uparrow\uparrow\downarrow\downarrow$ states along the two high symmetry directions are marked by blue crosses, and the spin structures are sketched as insets. Local geometry of the Fe atoms (red) in fcc and hcp stacking shown as insets.

deep energy minima on the order of 10–15 meV/Fe atom for spin spirals with periods of $\lambda \approx 1.2$ nm. The origin of these spin spiral minima is frustration of exchange interactions, where the nearest-neighbor exchange interaction favors FM alignment, but second or third nearest-neighbor exchange interactions are AFM (for exchange constants, see Ref. [33]).

Including SOC, see red data in Fig. 1(b), leads to a preference of right-rotating cycloidal spin spirals due to DMI for both types of stacking of the Rh overlayer. However, the energy differences are relatively small compared to the depths of the spin spiral energy minima neglecting SOC.

Because a significant role of higher-order exchange interactions has been reported for the Fe/Rh [31,32] and Fe/Ir [20] interfaces, we have also considered collinear $\uparrow\uparrow\downarrow\downarrow$ states along the high symmetry directions. These states are formed by the superposition of spin spirals and should be energetically degenerate with them within the Heisenberg model. Energy differences obtained within DFT indicate higher-order exchange contributions [28]. For fcc-Rh we find that both $\uparrow\uparrow\downarrow\downarrow$ states have a higher energy compared to the respective spin spirals, and the magnetic ground state remains a spin spiral along $\overline{\Gamma M}$ [Fig. 1(b)] [46]. For hcp-Rh we find that the $\uparrow\uparrow\downarrow\downarrow$ state along the $\overline{\Gamma K}$ direction is about 34 meV/Fe atom higher than the FM state; however, the $\uparrow\uparrow\downarrow\downarrow$ state along the $\overline{\Gamma M}$ direction is by about 12 meV/Fe atom lower in energy than the lowest spin spiral state [Fig. 1(b)]. The origin of the stacking-dependent magnetic ground state lies in the symmetry of Fe between the Rh and Ir layers [insets of Fig. 1(b)], which significantly modifies the electronic structure (see Ref. [33]).

When a magnetic tip is used in STM, the tunnel magnetoresistance (TMR) effect occurs, which leads to a spin-polarized contribution to the tunnel current in addition to the structural and electronic signal [47,48]. Figure 2(a) shows such an SP-STM measurement of a fcc-Rh/Fe island exhibiting a cosinelike magnetic modulation with a period $\lambda_{\mathrm{fcc}} \approx 1.5$ nm [see Fig. 2(b)] and propagation along $\langle 11\bar{2}\rangle$ directions. We conclude that fcc-Rh/Fe exhibits a spin spiral ground state with a continuous rotation of adjacent magnetic moments (see Ref. [33] for further measurements), in agreement with the spin spiral found along the $\overline{\Gamma M}$ direction from DFT [cf. Fig. 1(b)].

The SP-STM image in Fig. 2(c) shows a hcp-Rh/Fe island, and a similar stripe pattern with a slightly smaller period ($\lambda_{\mathrm{hcp}} \approx 1.1$ nm) is visible. The magnetic structure differs from the one in fcc-Rh/Fe islands in subtle aspects: the propagation direction seems to be more flexible, it is not strictly along $\langle 11\bar{2}\rangle$ directions but instead varies locally; the shape of the periodic signal significantly differs from a cosine, compare profile in Fig. 2(d). This demonstrates that the magnetic ground state of the hcp-Rh/Fe island is different from that of fcc-Rh/Fe.

Because in STM several different magnetoresistive (MR) effects can contribute to the measurement signal [49,50], in Fig. 2(e) we use a non-spin-polarized tip to separate purely electronic contributions from signal variations due to the TMR. We find that for fcc- and hcp-Rh the TMR signals with periods of about 1.5 and 1.1 nm, respectively, vanish. On fcc-Rh on Fe/Ir(111) no remaining modulation of the signal is observed in the bias voltage regime ± 1 V. In contrast, the non-spin-polarized signal observed on hcp-Rh is rather strong, i.e., on the order of a few pm, with half of the magnetic period, see Fig. 2(e), and can be observed in a bias voltage regime of around ± 0.2 V.

In the Tersoff-Hamann model [51] and its spin-polarized version [52], the STM image corresponds to the (spin-resolved) local vacuum density of states (LDOS) and can be calculated via DFT. First we consider a non-spin-polarized tip. The calculated STM image of hcp-Rh/Fe/Ir(111) in

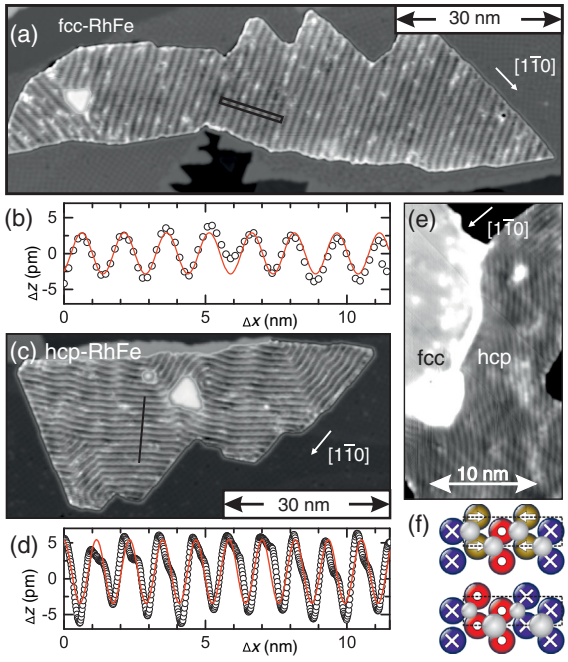

FIG. 2. (a),(c) SP-STM constant-current images of a fcc-Rh and a hcp-Rh island on Fe/Ir(111), respectively, measured with a magnetic Cr tip, sensitive to the out-of-plane magnetization component of the sample (contrast level adjusted locally on the Rh/Fe to ±20 pm; $T = 8$ K, $U = +30$ and -30 mV, $I = 1.0$ and 1.5 nA, respectively). (b),(d) Line profiles along the rectangles in (a) and (c); solid lines are fits with cosine functions. (e) Constant-current STM image of a Rh island with fcc and hcp stacking on fcc-Fe/Ir(111) measured with a non-spin-polarized tip (contrast ±15 pm; $T = 8$ K, $U = +15$ mV, $I = 6$ nA). (f) Top-view sketches of a homogeneous 4 atom period spin spiral and of the ↑↑↓↓ state; the bottom layer shows the Fe atoms and color and symbols indicate their magnetization directions; the top layer shows the Rh atoms and their size indicates the magnitude of their induced moments. The magnetic unit cells are indicated by the dotted boxes.

the ↑↑↓↓ state [Fig. 3(a)] shows a stripe pattern with half the magnetic period as in the experiment [Fig. 2(e)], and the corrugation amplitude amounts to a few picometer (pm) [Fig. 3(c)]. In the ↑↑↓↓ state the Rh atoms are inequivalent with different magnetic moments depending on whether the moments of all three neighboring Fe atoms are parallel ($m^{\mathrm{hcp}}_{\mathrm{Rh1}} = \pm 0.43\mu_B$) or two are parallel and one is antiparallel ($m^{\mathrm{hcp}}_{\mathrm{Rh2}} = \pm 0.08\mu_B$). Thereby, the magnetic structure of the Fe layer is imposed on the Rh surface layer. A similar effect has been predicted previously for STM images of an Fe monolayer on Rh(111) [32]. For hcp-Rh/Fe/Ir(111) investigated here it is stronger, as it stems from the Rh layer which is at the surface (see Ref. [33] for cross-sectional plots). In contrast, in the spin spiral state all Rh atoms are equivalent [see Fig. 2(f)] and the magnetic structure does not show up in STM images with nonmagnetic tips [cf. Fig. 2(e)]. The SP-STM image assuming a spin-polarized tip [Fig. 3(b)] shows a stripe pattern with the magnetic period of the ↑↑↓↓ state. Note that the inequivalent LDOS of the Rh surface atoms leads to a different spin contrast above the Fe atoms with parallel magnetic moments (see Ref. [33] for cross-sectional plots). The scan lines display an asymmetric shape [Fig. 3(c)], as in the experiment.

To investigate experimentally whether the hcp-Rh/Fe exhibits a strictly collinear magnetic ground state, we image the out-of-plane and the in-plane magnetization components of the same island; see Figs. 4(a) and 4(b), respectively. This is done by using an Fe-coated W tip that aligns its magnetization in out-of-plane magnetic fields whereas it has a magnetization in the surface plane without external magnetic field. Figure 4(a) demonstrates that in measurements with an out-of-plane sensitive tip, all three rotational domains appear the same; the pattern consists of slim bright lines spaced with the magnetic periodicity. Such a pattern is observed when the magnetic and the electronic MR contributions are of similar magnitude and in phase; i.e., the magnetic maxima (minima) coincides with the maxima of the electronic contribution and thus add up (cancel) [53].

The SP-STM image with in-plane magnetized tip in Fig. 4(b) shows a qualitatively different pattern in the central rotational domain compared to the two other rotational domains. This means that there are also magnetic in-plane components in the sample; given that the spin texture is of cycloidal nature due to the DMI, we can derive a tip magnetization axis as indicated, leading to a large magnetic contribution to the signal for the central domain. The

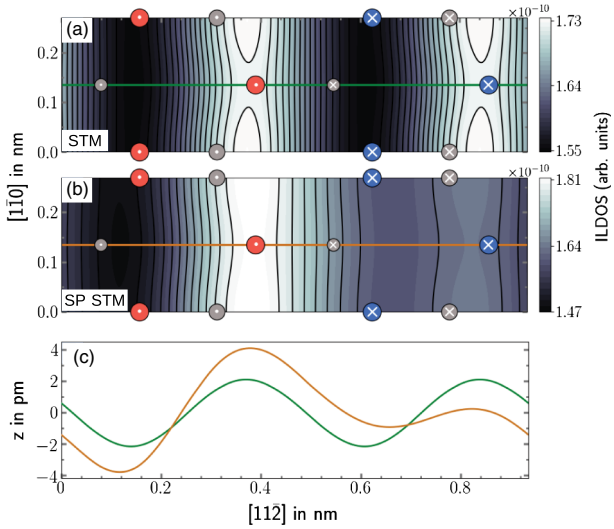

FIG. 3. STM images calculated based on DFT for hcp-Rh/Fe/Ir(111) in the ↑↑↓↓ state along $\overline{\Gamma M}$. (a) STM image at a distance of $z = 6.7$ Å for a non-spin-polarized tip. (b) SP-STM image for a tip spin polarization of 0.5. Red and blue circles denote Fe atoms. Gray circles indicate Rh atoms and their size the magnitude of magnetic moments. Dots and crosses denote upward and downward moments. (c) Line scans along the [11$\bar{2}$] direction for the images in (a) (green line) and in (b) (orange line). The integrated LDOS (ILDOS) has been calculated between the Fermi energy E_F and $E_F - 0.1$ eV.

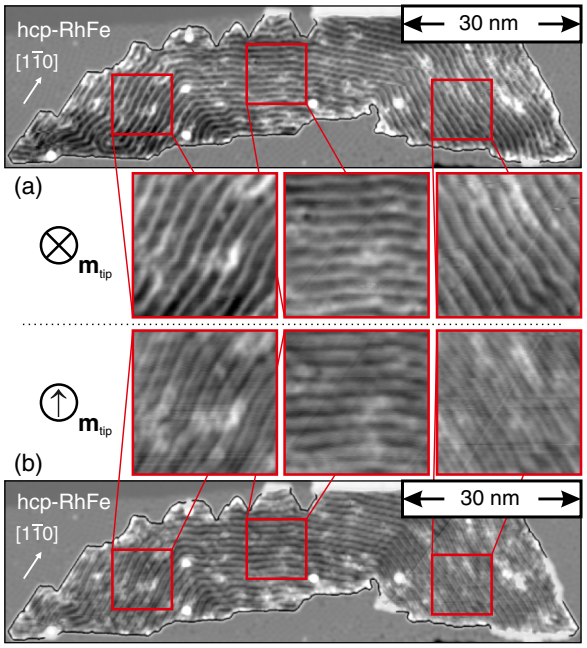

FIG. 4. (a),(b) Constant-current SP-STM images of a hcp-Rh island on Fe/Ir(111) measured with out-of-plane sensitive and in-plane sensitive magnetic Fe-coated W tip, respectively; the tip magnetization $\mathbf{m}_{tip}$ aligns in the applied out-of-plane field of $B = -2$ T (a), but is in the sample surface plane without applied field (b); its direction as indicated is derived from comparison of the relative magnetic contrast amplitudes of the three symmetry-equivalent rotational domains, see enlarged images (all contrast levels adjusted locally to ± 15 pm) ($T = 8$ K, $U = +30$ mV, $I = 3$ nA).

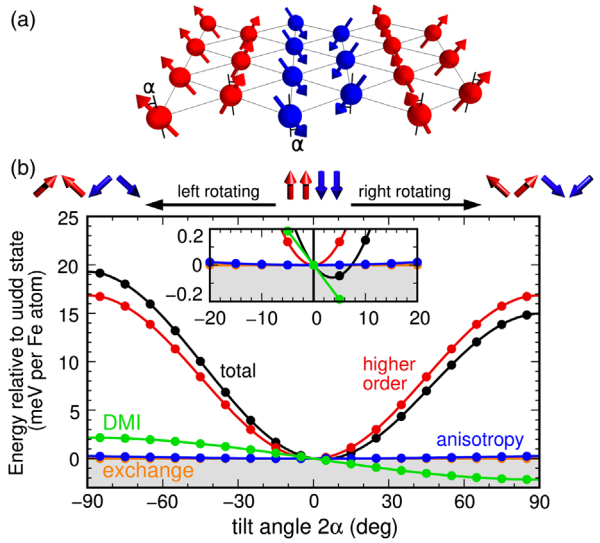

FIG. 5. (a) Sketch of the canted ↑↑↓↓ state defined by the angle α. Only the magnetic moments in the Fe layer are shown. Blue and red denote an upward or downward out-of-plane magnetization component. (b) Energy as a function of α resolved by the contributions from different magnetic interactions. The filled circles are obtained numerically using the DFT interaction parameters for the atomistic spin model and the lines are from the analytical forms of the contributions (see text). Note that a positive (negative) value of α indicates a clockwise (anticlockwise) rotation of the magnetic moments.

magnetic signal is small in the other two domains, and there the electronic contribution with half the magnetic period dominates the image. From these measurements we conclude that we have both out-of-plane as well as in-plane magnetization components in this sample and can thus rule out a strictly collinear ↑↑↓↓ state. However, because of the large electronic effect observed experimentally, which we attribute to the magnetic moment variation of the Rh atoms, we propose that the hcp-Rh/Fe/Ir(111) realizes a magnetic state in between the two extreme cases of homogeneous spin spiral and ↑↑↓↓ [see Fig. 2(f)], i.e., an inhomogeneous spin spiral or a canted ↑↑↓↓ state. Because the periodic modulation of the LDOS as manifested in the electronic contrast also changes the spin polarization of the Rh atoms (see Fig. S9 of Ref. [33]), we cannot quantitatively compare the measured magnetic amplitudes to extract the canting angle.

The DFT calculations of Fig. 1(b) have considered homogeneous spin spirals and collinear ↑↑↓↓ states. To include inhomogeneous spin spirals, as found experimentally, and study which energy contributions could lead to such a state, we introduce a canting angle α relative to the easy out-of-plane magnetization axis; see Fig. 5(a). This allows us to continuously transform the ↑↑↓↓ state ($\alpha = 0°$) to the 90° clockwise spin spiral ($\alpha = 45°$). Negative values of α denote an anticlockwise spin canting. It can easily be shown that the exchange energy contribution does not depend on α. The magnetocrystalline anisotropy energy stabilizes the collinear state and varies as $E_{\mathrm{MAE}} \propto -\cos^2\alpha$; however, the MAE is small with 0.53 meV/Fe atom. The DMI favors a canting and decreases as $E_{\mathrm{DMI}} \propto -\sin 2\alpha$ for clockwise spin canting [Fig. 5(b)]. Note that the strength of the DMI and the MAE are obtained from DFT. The energy difference of about 17 meV/Fe atom between the ↑↑↓↓ and the 90° spin spiral state can only be due to higher-order exchange contributions since spin-orbit coupling has been turned off in the DFT calculation. This leads to a rise with $(1 - \cos^2\alpha)$ if we assume only nearest-neighbor four-spin and biquadratic interaction [see Eqs. (3) and (4) in Ref. [33]). The competition of DMI and these higher-order contributions leads to an energy minimum at $2\alpha \approx 4°$.

To check the validity of the spin model we have performed self-consistent noncollinear DFT calculations including spin-orbit coupling in the four atom per layer supercell of the ↑↑↓↓ state allowing the spins to relax to find the energetically most favorable state [54]. To make these calculations computationally feasible, we have considered a freestanding Rh/Fe/Ir trilayer, which is very similar to the Rh/Fe/Ir(111) film system in terms of its magnetic properties (see Ref. [33]). We find a canted ↑↑↓↓ state with $2\alpha \approx 7°$ energetically more favorable by

0.03 meV/Fe atom than the collinear ↑↑↓↓ state. Two of the Rh magnetic moments point almost perpendicular to the surface while the other two are at angles of about 13° with respect to the surface normal (see Fig. S7 [33]). Thus, the in-plane components are enhanced at the Rh surface layer, which explains the relatively strong in-plane contrast observed in SP-STM images (cf. Fig. S10 [33]).

In conclusion, we have shown that higher-order exchange interactions can play a decisive role in transition-metal trilayers and may compete with interfacial DMI. Our work demonstrates that higher-order exchange needs to be taken into account in the search for novel transition-metal interfaces potentially promising for complex noncollinear spin structures such as Skyrmions.

This work has received financial support by the European Union via the Horizon 2020 research and innovation programme under Grant Agreement No. 665095 (FET-Open project MagicSky), and by the Deutsche Forschungsgemeinschaft via SFB668-A8. We gratefully acknowledge computing time at the supercomputer of the North-German Supercomputing Alliance (HLRN).

Note added in proof.—An ↑↑↓↓ state has recently been observed in Fe/Rh(111) [55].

*kbergman@physnet.uni-hamburg.de

[1] I. E. Dzyaloshinskii, Sov. Phys. JETP **5**, 1259 (1957).
[2] T. Moriya, Phys. Rev. **120**, 91 (1960).
[3] A. N. Bogdanov and D. A. Yablonskii, Sov. Phys. JETP **68**, 101 (1989).
[4] A. N. Bogdanov and U. K. Rößler, Phys. Rev. Lett. **87**, 037203 (2001).
[5] S. Mühlbauer, B. Binz, F. Jonietz, C. Pfleiderer, A. Rosch, A. Neubauer, R. Georgii, and P. Böni, Science **323**, 915 (2009).
[6] X. Z. Yu, Y. Onose, N. Kanazawa, J. H. Park, J. H. Han, Y. Matsui, N. Nagaosa, and Y. Tokura, Nature (London) **465**, 901 (2010).
[7] S. Seki, X. Z. Yu, S. Ishiwata, and Y. Tokura, Science **336**, 198 (2012).
[8] A. Fert, V. Cros, and J. Sampaio, Nat. Nanotechnol. **8**, 152 (2013).
[9] N. Nagaosa and Y. Tokura, Nat. Nanotechnol. **8**, 899 (2013).
[10] R. Wiesendanger, Nat. Rev. Mater. **1**, 16044 (2016).
[11] M. Bode, M. Heide, K. von Bergmann, P. Ferriani, S. Heinze, G. Bihlmayer, A. Kubetzka, O. Pietzsch, S. Blügel, and R. Wiesendanger, Nature (London) **447**, 190 (2007).
[12] P. Ferriani, K. von Bergmann, E. Y. Vedmedenko, S. Heinze, M. Bode, M. Heide, G. Bihlmayer, S. Blügel, and R. Wiesendanger, Phys. Rev. Lett. **101**, 027201 (2008).
[13] S. H. Phark, J. A. Fischer, M. Corbetta, D. Sander, K. Nakamura, and J. Kirschner, Nat. Commun. **5**, 5183 (2014).
[14] A. Kubetzka, O. Pietzsch, M. Bode, and R. Wiesendanger, Phys. Rev. B **67**, 020401 (2003).
[15] M. Heide, G. Bihlmayer, and S. Blügel, Phys. Rev. B **78**, 140403 (2008).
[16] S. Meckler, N. Mikuszeit, A. Pressler, E. Y. Vedmedenko, O. Pietzsch, and R. Wiesendanger, Phys. Rev. Lett. **103**, 157201 (2009).
[17] G. Chen, J. Zhu, A. Quesada, J. Li, A. T. N'Diaye, Y. Huo, T. P. Ma, Y. Chen, H. Y. Kwon, C. Won *et al.*, Phys. Rev. Lett. **110**, 177204 (2013).
[18] S. Emori, U. Bauer, S. Ahn, E. Martinez, and G. Beach, Nat. Mater. **12**, 611 (2013).
[19] K. Ryu, L. Thomas, S. Yang, and S. Parkin, Nat. Nanotechnol. **8**, 527 (2013).
[20] S. Heinze, K. von Bergmann, M. Menzel, J. Brede, A. Kubetzka, R. Wiesendanger, G. Bihlmayer, and S. Blügel, Nat. Phys. **7**, 713 (2011).
[21] N. Romming, C. Hanneken, M. Menzel, J. E. Bickel, B. Wolter, K. von Bergmann, A. Kubetzka, and R. Wiesendanger, Science **341**, 636 (2013).
[22] N. Romming, A. Kubetzka, C. Hanneken, K. von Bergmann, and R. Wiesendanger, Phys. Rev. Lett. **114**, 177203 (2015).
[23] G. Chen, A. Mascaraque, A. T. N'Diaye, and A. K. Schmid, Appl. Phys. Lett. **106**, 242404 (2015).
[24] W. Jiang, P. Upadhyaya, W. Zhang, G. Yu, M. B. Jungfleisch, F. Y. Fradin, J. E. Pearson, Y. Tserkovnyak, K. L. Wang, O. Heinonen *et al.*, Science **349**, 283 (2015).
[25] O. Boulle, J. Vogel, H. Yang, S. Pizzini, D. de Souza Chaves, A. Locatelli, T. O. Mente, A. Sala, L. D. Buda-Prejbeanu, O. Klein *et al.*, Nat. Nanotechnol. **11**, 449 (2016).
[26] C. Moreau-Luchaire, C. Moutafis, N. Reyren, J. Sampaio, C. A. F. Vaz, N. Van Horne, K. Bouzehouane, K. Garcia, C. Deranlot, P. Warnicke *et al.*, Nat. Nanotechnol. **11**, 444 (2016).
[27] S. Woo, K. Litzius, B. Krüger, M.-Y. Im, L. Caretta, K. Richter, M. Mann, A. Krone, R. M. Reeve, M. Weigand *et al.*, Nat. Mater. **15**, 501 (2016).
[28] P. Kurz, G. Bihlmayer, K. Hirai, and S. Blügel, Phys. Rev. Lett. **86**, 1106 (2001).
[29] Y. Yoshida, S. Schröder, P. Ferriani, D. Serrate, A. Kubetzka, K. von Bergmann, S. Heinze, and R. Wiesendanger, Phys. Rev. Lett. **108**, 087205 (2012).
[30] M. Hoffmann, J. Weischenberg, B. Dupé, F. Freimuth, P. Ferriani, Y. Mokrousov, and S. Heinze, Phys. Rev. B **92**, 020401(R) (2015).
[31] B. Hardrat, A. Al-Zubi, P. Ferriani, S. Blügel, G. Bihlmayer, and S. Heinze, Phys. Rev. B **79**, 094411 (2009).
[32] A. Al-Zubi, G. Bihlmayer, and S. Blügel, Phys. Status Solidi B **248**, 2242 (2011).
[33] See Supplemental Material http://link.aps.org/supplemental/10.1103/PhysRevLett.120.207201 for experimental and computational details, which includes Refs. [34–45].
[34] K. von Bergmann, S. Heinze, M. Bode, E. Y. Vedmedenko, G. Bihlmayer, S. Blügel, and R. Wiesendanger, Phys. Rev. Lett. **96**, 167203 (2006).
[35] O. Pietzsch, A. Kubetzka, D. Haude, M. Bode, and R. Wiesendanger, Rev. Sci. Instrum. **71**, 424 (2000).
[36] M. Müller, K. Albe, C. Busse, A. Thoma, and T. Michely, Phys. Rev. B **71**, 075407 (2005).
[37] www.flapw.de.
[38] M. De Santis, Y. Gauthier, H. C. N. Tolentino, G. Bihlmayer, S. Blügel, and V. Langlais, Phys. Rev. B **75**, 205432 (2007).

[39] S. H. Vosko, L. Wilk, and M. Nusair, Can. J. Phys. **58**, 1200 (1980).
[40] B. Dupé, M. Hoffmann, C. Paillard, and S. Heinze, Nat. Commun. **5**, 4030 (2014).
[41] M. Heide, G. Bihlmayer, and S. Blügel, Physica (Amsterdam) **404B**, 2678 (2009).
[42] B. Zimmermann, M. Heide, G. Bihlmayer, and S. Blügel, Phys. Rev. B **90**, 115427 (2014).
[43] J. H. Mentink, M. V. Tretyakov, A. Fasolino, M. I. Katsnelson, and T. Rasing, J. Phys. Condens. Matter **22**, 176001 (2010).
[44] K. von Bergmann, M. Menzel, A. Kubetzka, and R. Wiesendanger, Nano Lett. **15**, 3280 (2015).
[45] A. K. Nandy, N. S. Kiselev, and S. Blügel, Phys. Rev. Lett. **116**, 177202 (2016).
[46] With an external magnetic field, a Skyrmion lattice phase can in principle be induced as shown by spin dynamics simulations (see Ref. [33]); however, due to the deep energy minimum, the transition fields are about 50 T.
[47] M. Bode, Rep. Prog. Phys. **66**, 523 (2003).
[48] R. Wiesendanger, Rev. Mod. Phys. **81**, 1495 (2009).
[49] M. Bode, S. Heinze, A. Kubetzka, O. Pietzsch, X. Nie, G. Bihlmayer, S. Blügel, and R. Wiesendanger, Phys. Rev. Lett. **89**, 237205 (2002).
[50] C. Hanneken, F. Otte, A. Kubetzka, B. Dupé, N. Romming, K. von Bergmann, R. Wiesendanger, and S. Heinze, Nat. Nanotechnol. **10**, 1039 (2015).
[51] J. Tersoff and D. R. Hamann, Phys. Rev. B **31**, 805 (1985).
[52] D. Wortmann, S. Heinze, P. Kurz, G. Bihlmayer, and S. Blügel, Phys. Rev. Lett. **86**, 4132 (2001).
[53] K. von Bergmann, M. Menzel, D. Serrate, Y. Yoshida, S. Schröder, P. Ferriani, A. Kubetzka, R. Wiesendanger, and S. Heinze, Phys. Rev. B **86**, 134422 (2012).
[54] P. Kurz, F. Förster, L. Nordström, G. Bihlmayer, and S. Blügel, Phys. Rev. B **69**, 024415 (2004).
[55] A. Krönlein *et al.*, following Letter, Phys. Rev. Lett. **120**, 207202 (2018).